High Kinetic Energy Ion Mobility Spectrometry- Mass Spectrometry investigations of four inhalation anaesthetics : isoflurane, enflurane, sevoflurane and desflurane

Weiss, Florentin

2022-05

Weiss , F , Schaefer , C , Ruzsanyi , V , Maerk , T , Eiceman , G , Mayhew , C A & Zimmermann , S 2022 , ' High Kinetic Energy Ion Mobility Spectrometry- Mass Spectrometry investigations of four inhalation anaesthetics : isoflurane, enflurane, sevoflurane and desflurane ' , International Journal of Mass Spectrometry , vol. 475 , 116831 . https://doi.org/10.1016/j.ijms.2022.116

http://hdl.handle.net/10138/343963
https://doi.org/10.1016/j.ijms.2022.116831

International Journal of Mass Spectrometry 475 (2022) 116831

Contents lists available at ScienceDirect

International Journal of Mass Spectrometry

journal homepage: www.elsevier.com/locate/ijms

High Kinetic Energy Ion Mobility Spectrometry – Mass Spectrometry investigations of four inhalation anaesthetics: isoflurane, enflurane, sevoflurane and desflurane

Florentin Weiss [a, b, *], Christoph Schaefer [c], Veronika Ruzsanyi [a, b], Tilmann Märk [d], Gary Eiceman [e, f], Chris A. Mayhew [a, b], Stefan Zimmermann [c]

[a] Institute for Breath Research, University of Innsbruck, Innsbruck, Austria
[b] Tiroler Krebsforschungsinstitut Innsbruck, Innsbruck, Austria
[c] Institute of Electrical Engineering and Measurement Technology, Leibniz University Hannover, Hannover, Germany
[d] Institute for Ion Physics and Applied Physics, University of Innsbruck, Innsbruck, Austria
[e] Department of Chemistry and Biochemistry, New Mexico State University, Las Cruces, NM, 88003, United States
[f] VERIFIN, Finnish Institute for the Verification of the Chemical Weapons Convention, Department of Chemistry, University of Helsinki, FI-00014, Helsinki, Finland

ARTICLE INFO

Article history:
Received 17 January 2022
Received in revised form
21 February 2022
Accepted 25 February 2022
Available online 2 March 2022

Keywords:
High Kinetic Energy-Ion Mobility Spectrometry
Proton Transfer Reaction-Time-of-Flight –Mass Spectrometry
Isoflurane
Enflurane
Desflurane
Sevoflurane

ABSTRACT

Here we report the first High Kinetic Energy-Ion Mobility Spectrometry-Mass Spectrometric (HiKE-IMS-MS) investigations involving four fluranes; isoflurane, enflurane, sevoflurane and desflurane. Unlike standard (atmospheric pressure) IMS, HiKE-IMS can detect these compounds in positive ion mode. This is because its low-pressure environment (~ 14 mbar) and the associated short ion drift times in the HiKE-IMS ensure the reagent ions $O_2^{+\bullet}$ and H_3O^+ are present in the reaction region, and these can react with the fluranes by dissociative charge and proton transfer, respectively. However, their ion intensities are very dependent on the value of the reduced electric field (*E/N*) applied and the humidity of the air in the reaction region of the HiKE-IMS. In this paper we explore the potential use of HiKE-IMS for air quality control and breath analysis of fluranes. To help in the interpretation of the ion mobility spectra, and hence the ion-flurane chemistry occurring in reaction region, a HiKE-IMS was coupled to a Time-of-Flight Mass Spectrometer so that the *m/z* values of both the reagent and product ions that are contained within the various ion mobility peaks observed could be identified with a high level of confidence. The dependencies of the intensities of these ions as functions of *E/N* (30–115 Td) and humidity in the reaction region are reported. A number of product ions have been observed only under low humidity conditions (H_2O volume-mixing ratio ~ 100 ppm_v), including CHF_2^+ and $CHFCl^+$ for isoflurane and enflurane, CHF_2^+, CF_3^+ and $C_3H_2F_5O^+$ for desflurane, and CH_3O^+, CHF_2^+, $C_3H_3F_4O^+$, $C_4H_3F_6O^+$ and $C_4H_3F_6O^+(H_2O)$ for sevoflurane. It is interesting to note that CH_3O^+, CHF_2^+, $CHFCl^+$ and CF_3^+ have shorter drift times than that measured for $O_2^{+\bullet}$. This is explained by resonant charge transfer reaction processes occurring in the drift region: $O_2^{+\bullet} + O_2 \rightleftharpoons O_2^{+\bullet}.O_2 \rightleftharpoons O_2 + O_2^{+\bullet}$.

1. Introduction

Fluranes are common inhalation anaesthetics that are widely used in surgery. These include, among others, the following three highly volatile halogenated ethers: isoflurane ($C_3H_2ClF_5O$), which currently is the one most commonly used worldwide, desflurane ($C_3H_2F_6O$) and sevoflurane ($C_4H_3F_7O$) [1]. Enflurane is now rarely used as an inhalation anaesthetic, but, being a structural isomer of isoflurane, it is of interest to include it in this study for comparison with the reagent ion-isoflurane chemistry.

A possible biochemical pathway for the metabolism of isoflurane has been reported by Hitt *et al* [2], with it being metabolized to trifluoroacetic acid (CF_3CO_2H), HF and CO_2. Sevoflurane is considered to be metabolized in renal tissue cells by the isoenzymes cytochrome P_{450} 2A1, 2A6 and 3A4, and hepatically by

* Corresponding author. Institute for Breach Research, University of Innsbruck, Innrain 66, A-6020, Innsbruck, Austria.
E-mail address: florentin.weiss@uibk.ac.at (F. Weiss).

https://doi.org/10.1016/j.ijms.2022.116831

P_{450} 2E1 to hexafluoro-2-propanol [3]. However, the metabolization rates of the fluranes are very low, resulting in low metabolism; isoflurane ≈ 0.3%, enflurane ≈ 2–5%, desflurane ≈ 0.02–0.03%, and sevoflurane ≈ 3–6% [3]. The major loss of these fluranes from the body is through urination and exhalation. Hence, after surgery, an halogenated anaesthetic remains in a person's blood for some time, with a fraction becoming stored in fat (tissue uptake) according to the blood-fat partition coefficient, $\lambda_{blood:fat}$ [4]. The part of the anaesthetic that remains in the blood will be delivered to the lungs by the systemic circulation. Diffusion from the blood to the breath occurs, and the alveolar breath concentration will therefore be dependent on the solubility of the anaesthetic in blood, which is expressed by the blood-air partition coefficient $\lambda_{blood:air}$ [5]. The actual concentration of a given anaesthetic in end-tidal breath will be directly related to the alveolar concentration and hence indirectly to blood concentrations. Thus, an analysis of exhaled breath provides a method to determine the levels of these compounds circulating in the human body, and temporal measurements can be used to investigate their washout characteristics (the so-called pharmacokinetics) from the body. The clearance of a flurane out of the body will depend on many factors such as a patient's health, body-mass-index, type of ventilation during surgery, and the duration of the surgery [4]. In addition, any premedication before the administration of an inhaled anaesthetic can also affect the washout, as has been shown in a study involving morbidly obese patients [6].

Ideally, exhaled breath volatiles should be analysed in real-time to limit sampling issues. Another, and perhaps more important, application for the real-time monitoring of inhalation anaesthetics is for determining occupational health exposure in medical settings (e.g., in operating theatres and post-anaesthetic care units) [7]. One analytical technique that is well proven for the detection of breath volatiles in clinical environments is Proton Transfer Reaction–Mass Spectrometry, PTR-MS [8–13]. Using PTR-Time-of-Flight-MS (PTR-TOF-MS), Malásková *et al* investigated in detail the reactions of H_3O^+ with the four fluranes associated with this study, with that investigation focussing on the potential real-time monitoring of volatile halogenated anaesthetics in breath [14]. For that study the reagent ions were generated via a series of ion-molecule reactions following an electrical discharge in a hollow cathode containing a mixture of air and water [15]. Upon entering the drift (reaction) region, these reagent ions reacted with trace levels of the individual fluranes introduced in trace quantities (~ 400–500 parts per billion by volume (ppb_v)) via an air carrier gas flow into the front-end of the drift tube. At the end of the drift tube, a fraction of the reagent and product ions entered the TOF-MS for analysis to determine their mass-to-charge ratios (*m/z*) [16]. The dependence of the product ion distributions on the reduced electric field (*E/N*), which is the ratio of the electric field (*E*) to the buffer gas density (*N*) in the drift tube, was investigated over a range from 80 to 220 Td (where 1 Td = 10^{-21} V m^2). The product ions identified in that PTR-TOF-MS study with high intensities were $CHFCl^+$(*m/z* 66.98) for isoflurane and enflurane, $C_3H_2F_5O^+$(*m/z* 149.00) for desflurane, and $C_4H_3F_6O^+$(*m/z* 181.01) for sevoflurane, with all the *m/z* values being given for the lightest isotopomer. Earlier studies involving lower mass resolution PTR-quadrupole-MS and Selected Ion Flow Tube Mass Spectrometer (SIFT-MS) systems investigated the reactions of H_3O^+ with sevoflurane [17]. $C_4F_7OH_2^+$ was mainly found in the PTR-quadrupole-MS study, while $C_4F_6H_2OH^+$ was predominantly found in the SIFT-MS investigation. Another SIFT-MS study reported the ion chemistry of H_3O^+ and $O_2^{+\bullet}$ with sevoflurane and isoflurane [18].

Although PTR-TOF-MS and SIFT-MS are ideal for discovery studies and excellent analytical tools in a research environment, they are both expensive and complex analytical tools that are unsuitable for routine point-of-care (PoC) clinical measurements. Ion Mobility Spectrometry (IMS) is better suited for this owing to its good detection limits (double-digit parts per trillion by volume (ppt_v) range) and portability, being also available in miniaturized form, as shown by Ahrens *et al* [19]. In addition, IMS does not require major training to use, so that PoC applications become straightforward for medical staff, although certain PTR-MS applications nowadays also run automatically.

A recent development in IMS is High Kinetic Energy-Ion Mobility Spectrometry (HiKE-IMS), as described first by Langejuergen *et al* [20]. Here we investigate its potential analytical application for detecting the four inhalation anaesthetics in positive polarity mode, under relatively dry buffer gas conditions, e.g., for use in determining air quality in operating theatres or in recovery rooms, and under more humid conditions, e.g., for use in volatile breath analysis.

Unlike a classic IMS system, which operates at just above the pressure of the atmosphere where the instrument is located, the HiKE-IMS is operated at much lower pressures of between 10 and 40 mbar. Therefore, using typical atmospheric pressure IMS drift tube voltages, *E/N* strengths up to 120 Td can be readily reached in the HiKE-IMS, making it comparable to those used in standard PTR-TOF-MS operation, but at much lower instrumental size and cost. However, unlike PTR-TOF-MS, for which H_3O^+ is the dominant reagent ion over a large *E/N* range, with HiKE-IMS operating in air a number of reagent ions are observed to be present with significant intensities, namely (and in order of observed drift times (see later)), $NO^+(H_2O)_m$ (m = 0 and 1), $H_3O^+(H_2O)_n$ (n = 0, 1, 2 and 3) and $O_2^{+\bullet}$ [21–23]. Their relative intensities and the cluster sizes depend not only on the value of *E/N*, which determines the ion-neutral collisional energies and the reaction/drift times of the ions, but also of course on the humidity of the air in the drift tube. For fixed *E/N* (and hence fixed reaction/drift times) clustering with water molecules increases with increasing humidity in both the reaction and drift regions [24].

To determine the potential analytical application of HiKE-IMS to detect the four specified fluranes, either in a room environment (e.g., in operating theatres or in post operation recovery rooms) or in exhaled breath, we report here details on their ion mobilities and identify the product ions as a function of *E/N* over a range of 30–120 Td under normal humidity operating conditions, ~ 0.5% relative humidity (rH), and higher humidity conditions, ~ 25% rH, for the inlet (sample) air flows entering the reaction region. The airflow in the drift region was maintained at ~ 0.5% rH for all measurements.

2. Methods

2.1. High Kinetic Energy - Ion Mobility Spectrometer (HiKE-IMS)

Information on the HiKE-IMS and its operating parameters have already been published in detail elsewhere [21,25]. Here we will only provide information pertinent to this study. In brief, the HiKE-IMS was operated at 14 mbar and maintained at just above room temperature (35 °C) using a temperature-controlled housing, with the sample gas inlet located opposite to its ionisation source, which is a corona discharge built in a point-plane design (corona needle APCI, Agilent Technologies) operating at 1300 V [21]. The drift gas is introduced into the HiKE-IMS near to the end of the drift tube. Both the drift and sample gases flow in the same direction, being pumped out of the instrument using a membrane pump (MVP 40, Pfeiffer Vacuum) connected to the front end (corona discharge region) of the HiKE-IMS. The outlet gas flow was controlled by an EVN-116 gas dosing valve (Pfeiffer Vacuum). A CMR-362 capacitive pressure gauge (Pfeiffer Vacuum) was used for monitoring the pressure in the drift tube (see Fig. 1 in Allers *et al* for clarification of

the positions of the membrane pump and the sample and drift gas inlets [26]).

The reaction and drift regions have lengths of 7.7 cm and 30.6 cm, respectively, with each having its own individual voltage supply to permit independent adjustment of the *E/N* values over the range of 30–120 Td. For this study, the *E/N* values were kept the same in both regions, but it should be appreciated that differing *E/N* can be applied to the separate sections in the drift tube, which could be used, for example, to manipulate the ion-chemistry in order to enhance analytical sensitivity and selectivity. Drift times in the reaction and drift regions are dependent on the value of *E/N*. In this study, the drift region *E/N* value was maintained at between 115 and 120 Td. This results in drift times for the reagent ions of between 300 and 400 μs, which is significantly less than the drifts times for IMS systems (typically tens of ms), and more comparable to the reaction (and drift) times associated with PTR-MS systems [16].

Sample and drift gases were connected via 250 μm inner diameter capillaries to the HiKE-IMS with lengths adjusted to provide 19 mL/min (millilitre standard per minute) flow rate (at reference conditions of 20 °C and 1013.25 hPa). The drift gas mixes within the reaction region with the sample gas. To provide purified dry air, a zero-air generator (JAG, JAGZAG600S) followed by a pressure swing absorber (Parker, K-MT 3 LAB), a moisture trap (<1 parts per million by volume (ppm_v) water) and a hydrocarbon filter were used. However, due to diffusion through various seals

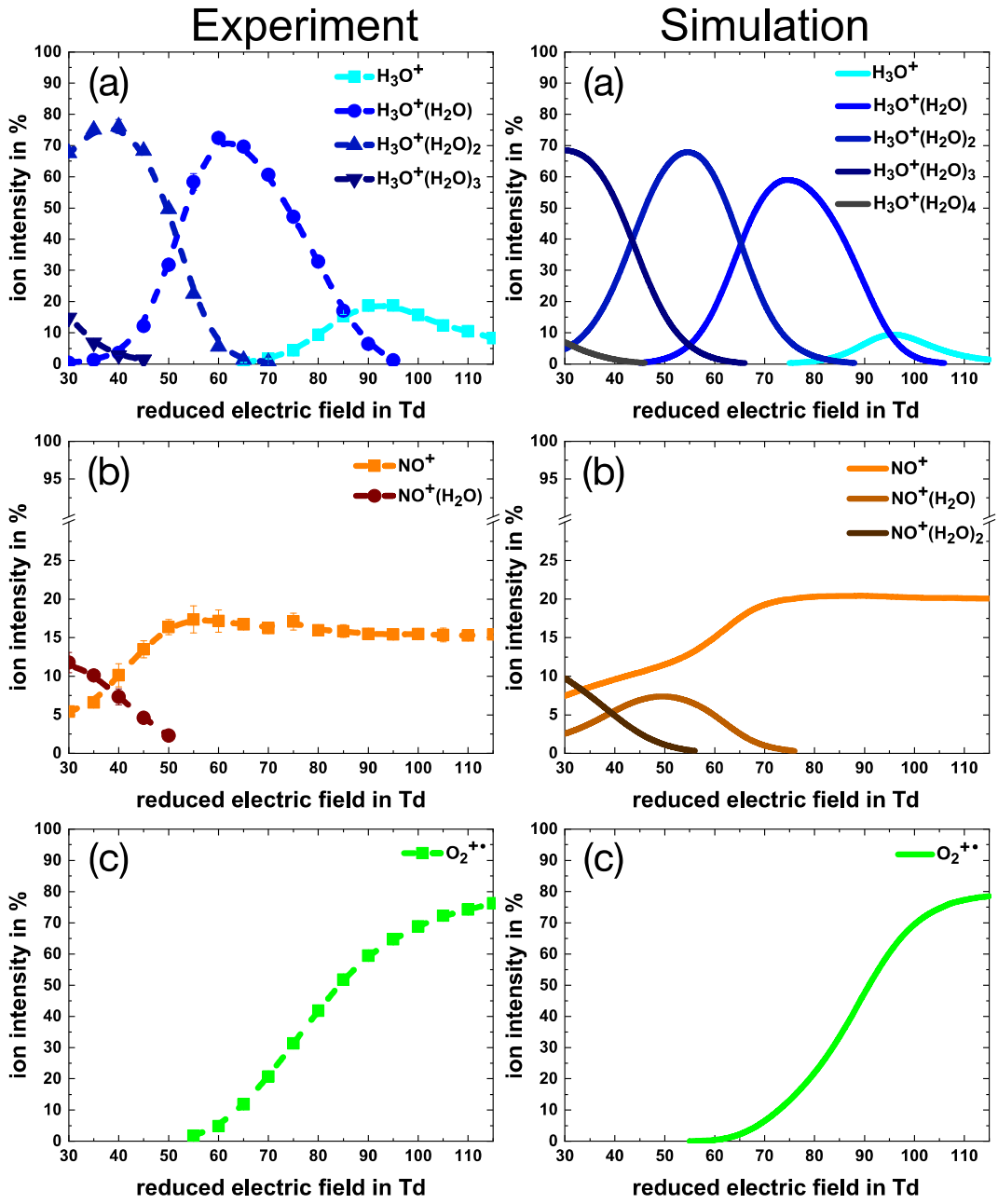

Fig. 1. HiKE-IMS-TOF-MS positive reagent ion percentage distributions for experimental (left side of figure) and simulated (right side of figure) values using dry (~ 100 ppm_v of H_2O) purified air for both the sample and drift gases as a function of *E/N*. For clarity, the three types of reagent ions, namely (a) $H_3O^+(H_2O)_n$ (n = 0, 1, 2, 3, and (only for the simulation) 4), (b) $NO^+(H_2O)_m$ (m = 0, 1 and (only for simulation) 2), and (c) $O_2^{+\bullet}$ are shown separately for ease of comparison. In determining the percentage distributions, no allowance has been made for any *m/z* transmission dependencies in the system.

and tubing, the residual water volume-mixing ratio in the HiKE-IMS significantly exceeds 1 ppm_v. To avoid variations in the HiKE-IMS, and for what we will define as normal operating (humidity) conditions, the humidity in the IMS was intentionally set to provide a H_2O volume-mixing ratio of ~ 100 ppm_v, providing a residual background water of ~ 0.5% rH. The measurements were then either carried out with this normal operating (relatively dry) air flow (~ 0.5% rH) for both the sample and drift gases, to mimic the conditions for potential analytical use in air quality control, or with a higher humid air flow into the reaction region (~ 25% rH), whilst retaining the normal operating drift gas humidity, in order to assess its value for breath-flurane measurements. The water volume-mixing ratio in the sample inlet airflow was varied by mixing the supplied purified air with purified air that was passed through a water container. With humid sample and normal operational drift air flows, the humidity of the air exhausting from the reaction region was measured to be ~ 2000 ppm_v (~ 10% rH), as measured by a dew point sensor (Michell Instruments, Easidew Transmitter). However, the humidity of the air in the reaction region of the HiKE-IMS is expected to be slightly lower than this value, because the humidity measurement was taken before the dew point sensor reached a stable signal (which can take days).

Reagent ions generated in the ionisation region and product ions created through reactions with the reagent ions in the reaction region migrated under the influence of the applied electric field towards an ion-gate. Using a square wave pulse of 1 μs width operating at a frequency of between 100 and 500 Hz, ions were pulsed into the drift region of the HiKE-IMS's drift tube. Ion currents were measured at the end of the drift region by using a Faraday plate that was connected to a fast current amplifier (Femto, DLPCA-200, 400 kHz, 1×10^7 V/A). These currents, recorded as a function of drift time, generated the ion mobility spectral profiles. The HiKE-IMS resolving power (R) varies from a maximum of about R = 140 at 120 Td to a minimum of approximately R = 80 at 30 Td.

For the mass spectrometric measurements a second HiKE-IMS of slightly different design from the one used to measure the ion mobility spectra was coupled to a self-built time-of-flight mass spectrometer (TOF-MS). This second HiKE-IMS contained a second ion-gate that had been incorporated into the instrument near to its three-gate construction at the end of the drift tube. This second ion gate was operated by being either (i) fully opened in order to allow a percentage of all of the ion types (reagents and products) continuously through to the ion transfer region and then into the mass spectrometer or (ii) gated to allow ions that have a selected range of drift times through for *m/z* analysis in order to determine which ions are associated with a given ion mobility peak. The transmission efficiencies of the ions between the drift tube and the MS ion detection are very low, as is true for all IMS-MS systems in general, because only an extremely small percentage of ions will pass through to the detection region. This can be quantified by comparing the count rates per second for a given *m/z* in the mass spectra compared to its ion mobilty intensity (see results later). However, this is not an issue here for identifying the *m/z* of the ions given the sensitivity of the MS.

2.2. Ion transfer and time-of-flight-mass spectrometer regions

Details of the self-built TOF-MS and its coupling to the HiKE-IMS are provided by Allers *et al* [21]. In brief, a percentage of the reagent and product ions exited the drift tube region via a pinhole of 0.8 mm diameter that is at the centre of the three gate construction to enter the ion transfer region, which was maintained at a pressure of 3×10^{-3} mbar by using a turbo pump (Pfeiffer Vacuum, HiPace 300). The transferred ions were then drawn towards a skimmer cone, placed at a distance of 2 cm behind the Faraday plate, that itself contains a central hole of 1.0 mm diameter. Through this, the ions entered the TOF-MS detection region, which was operated at a pressure of 6×10^{-6} mbar, being maintained by the turbo pump used for the ion transfer region.

The TOF-MS consists of an orthogonal acceleration path, according to the Wiley-McLaren arrangement, a short linear field free flight path (28.5 cm), and a microchannel plate as the detector for the ions. The mass resolution ($m/\Delta m$) of the TOF-MS is low, being only approximately 80 at an *m/z* of about 100, but this is sufficient to provide reasonably accurate peak positions. Given that we know what volatile analyte is introduced into the system, the molecular formula of the product ions can usually be determined with little ambiguity. As mentioned above, depending on how the second HiKE-IMS ion-gate is used, two modes of recording mass spectra are possible, namely: **Total Ion Mode** (all types of ions transmitted through) or **Selected Ion Mode** (selected ions only transmitted within a given range of drift times). The spectrum-to-spectrum acquisition rate of the TOF-MS was set to 2 kHz.

For Total Ion Mode, both ion gates are left open, so that a percentage of the reagent and product ions present at the end of the drift tube is continuously transferred into the TOF-MS, as described by Allers *et al* [21]. A mass spectrum is acquired for a selected acquisition period (in this study 90 s was used) at fixed specified values of *E/N*. Once a mass spectrum is completed, the voltage across the drift region is increased to raise the *E/N* value, and another mass spectrum is recorded. In this way, for this study, mass spectra were recorded over an *E/N* range of 30—115 Td in steps of 5 Td, with three mass spectra being recorded and averaged for each *E/N* value. A Gaussian was fitted to each ion mass spectral peak, and the corresponding areas were averaged for each *E/N* value.

For Selected Ion Mode, only ions arriving at the second ion-gate with a pre-defined range of drift times were injected into the TOF-MS, allowing the recording of mass spectra associated only with specified ion mobility regions (full peaks or selected parts of peaks for which shoulders are present). This was achieved by pulsing the first gate and then opening the second grid at the end of the drift region at a specific time after the first gate is opened and for a desired drift time interval. Thus, in this mode of operation, ions with specific *m/z* values could be assigned to specific regions in the ion mobility spectra.

2.3. Fluranes

Surgical grade inhalation anaesthetics were used for the present studies. Enflurane (CAS: 13838-16-9) was purchased from Abbott Products Operations AG, isoflurane (CAS: 26675-46-7) and sevoflurane (CAS: 28523-86-6) came from AbbVie, and desflurane (CAS: 57041-67-5) was sourced from Baxter International. All were used without further purification. Individual fluranes were introduced into the reaction region of the HiKE-IMS using a permeation tube placed inside the inlet line that is coupled to the reaction region. Permeation tubes were created from low-density polyethylene pipettes (Baxter International) and maintained at 35 ^oC in the inlet line. Diffusion through the permeation tubes, at known measured rates, provided sufficient flurane concentrations in the reaction region of the HiKE-IMS to provide good ion mobilty peaks and sufficient product ion intensities, but for which the reagent ion signals were still present. This was done in order to minimise possible secondary product ion-flurane reaction processes. Through this method, anaesthetics' volume-mixing ratios in the range of approximately 1.2—4.0 ppm_v were achieved. The higher concentration values were used for the mass spectrometric measurements in order to increase the product ion intensities for higher accuracy in the determination of their *m/z* values, and hence the identification of the product ions with a higher level of confidence.

Isotope ratios were also taken into account to aid in the identification of the product ions.

2.4. Simulation of the reagent ion populations in HiKE-IMS

To simulate the reagent ion populations at the end of the reaction region in the HiKE-IMS for fixed water concentration values as a function of *E/N*, a simple kinetic model was used, based on kinetic and thermodynamic data available in the literature. The kinetic modelling used for the simulations presented in this paper is described in detail in a previous work by Allers *et al* [26]. We also adopted the simplified reaction scheme used by Allers *et al* (see Fig. 2 of that paper). For this particular study, the following conditions were used. An initial signal percentage intensity of $NO^+(H_2O)_m$ (m = 0, 1, 2 and 3) to be 20% between 30 and 115 Td was applied for the simulation. This was based on the observation that this is the approximate measured percentage of $NO^+(H_2O)_m$ (m = 0 and 1) compared to the total reagent ion signals. $N_2^{+\bullet}$ and $O_2^{+\bullet}$ initial relative intensities were set to the same ratio as their corresponding neutral abundances found in air. This assumes that the ionisation efficiency for N_2 and O_2 in the corona discharge are the same and ignores the formation of $O^{+\bullet}$ and N^+ precursor ions. Thus, in summary, for the simulations, we started with the relative precursor ion abundances to be $N_2^{+\bullet} = 0.63$, $O_2^{+\bullet} = 0.17$ and $NO^+ = 0.2$. Using Van't Hoff's theorem [27], and the standard molar entropy and enthalpy change of the reactions, the rates of the back reactions were also determined. The effective ion temperature used in the reactions for specific *E/N* values was determined from the Wannier

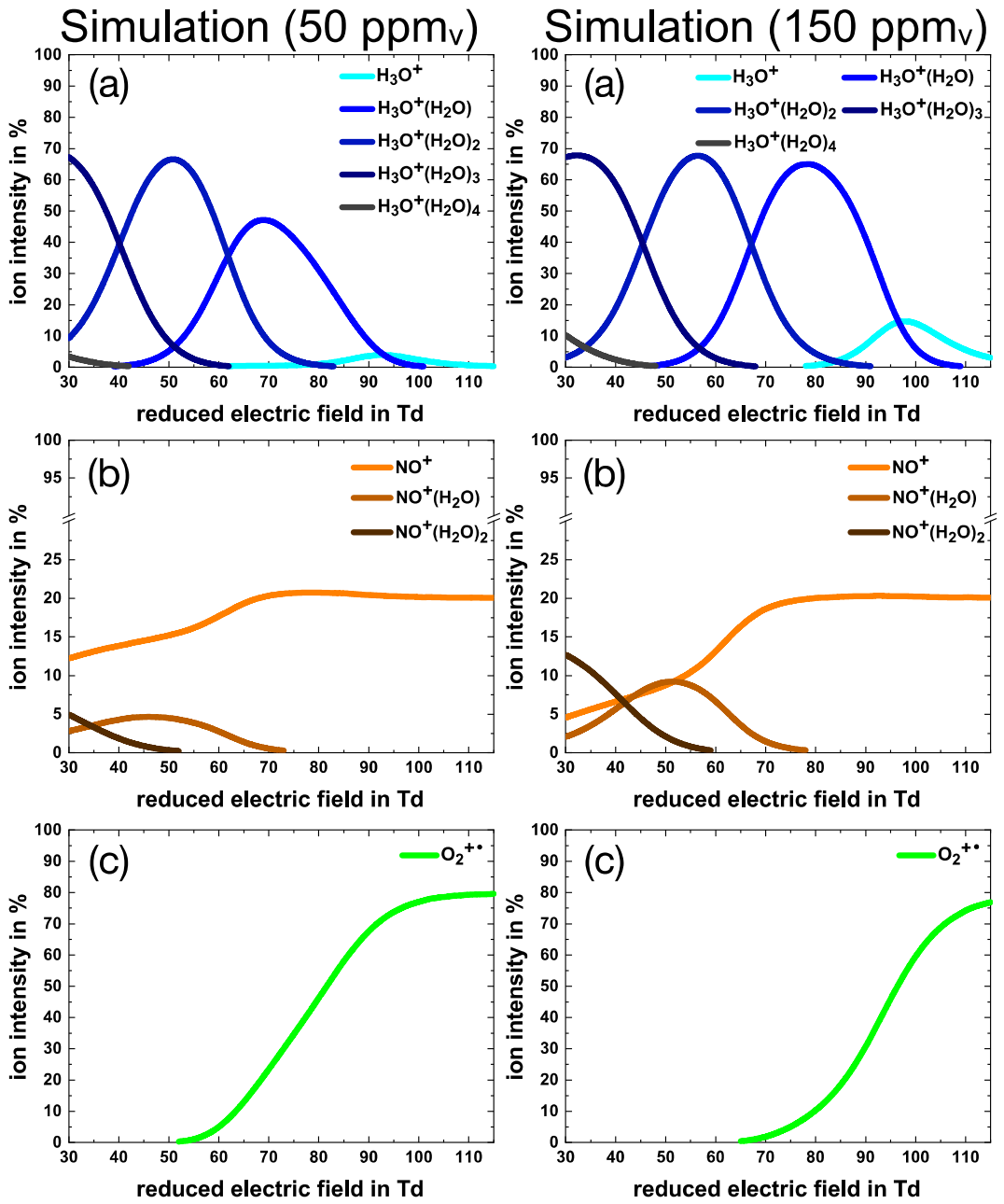

Fig. 2. Modelling the positive reagent ion concentrations in the HiKE-MS for (a) $H_3O^+(H_2O)_n$ (n = 0, 1, 2, 3, and 4), (b) $NO^+(H_2O)_m$ (m = 0, 1 and 2), and (c) $O_2^{+\bullet}$ for H_2O concentrations in the reaction region corresponding to volume-mixing ratios of 50 ppm_v (left side of figure) and 150 ppm_v (right side of figure) to demonstrate the sensitivities of the ion signal intensities for relatively small changes in water concentrations.

equation [28].

2.5. Density functional theory calculations

Density functional theory (DFT) calculations have been undertaken to determine for the first time the values for the changes in the gas-phase enthalpies (ΔH) and free energies (ΔG) of certain key ion-molecule reactions leading to the formation of the reagent ions (see equations (1) – (9) later). These calculations were conducted using the Gaussian09W program with the GaussView05 for Windows interface and the B3LYP functional with 6–31 + G(d,p) basis set at 298 K [29]. It should be noted that the translational temperature of the ions (the effective ion temperature) is higher than this due to the presence of the electric field (as expressed by the Wannier equation previously mentioned). However, this is not considered important, because the energetics are used only as a guide in this paper to help understand the key ion reaction processes.

3. Results and discussion

3.1. Reagent ion distributions as a function of E/N using "normal" operating (low humidity) air (H_2O volume-mixing ratio ~ 100 ppm_v) for both sample and drift gas flows

Compared to HiKE-IMS, for normal atmospheric pressure IMS systems operating in positive ion mode and using air as the buffer gas, the effect of the high pressure leads to an increased number of reactions per unit time and increased reaction (drift) times, which in turn leads to complete conversion of all the precursor ions (mainly $N_2^{+\bullet}$ and $O_2^{+\bullet}$, but also NO^+) to the terminal reagent ion species $H_3O^+(H_2O)_n$ (n = 0, 1, 2, 3, …). Together, these terminal $H_3O^+(H_2O)_n$ reagent ions result in just one dominating reagent ion peak (RIP) being observed in the ion mobility spectrum (ion current versus ion drift time) owing to their interconversion during transit through the drift region of the IMS's drift tube.

Compared to atmospheric pressure IMS instruments, under the operational parameters of the HiKE-IMS system, also operating in positive ion mode, the associated low reaction and drift regions' pressure and the decreased number of reactions and drift times lead to incomplete conversion of the precursor ions to the terminal ions, namely $H_3O^+(H_2O)_n$. This lack of ion conversion leads to three types of reagent ions being present in the reaction region of the drift tube, which in the mass spectra are measured to be $H_3O^+(H_2O)_n$ (n = 0, 1, 2, and 3), $NO^+(H_2O)_m$ (m = 0 and 1), and $O_2^{+\bullet}$, with their intensities being very much dependent on the *E/N* value for fixed humidity. When these ions are pulsed into the drift region, differences in their ion mobilities result in three well separated RIPs being measured in the ion mobility spectrum, as is illustrated in the paper by Allers *et al* (see Fig. 4 of that paper) [21]. In addition, in this study two other reagent ions, namely NO_2^+ and $O_4^{+\bullet}$, have also been detected. However, as these were found to have negligible intensities compared to the other reagent ions (typically <1% of the total reagent ion signal) they are not considered important for analytical purposes, and hence they will not be discussed in any detail in this paper. Although the presence of three types of reagent ions in the reaction region can make the ion chemistry involving a neutral analyte more complex than would occur in high pressure IMS systems, their simultaneous presence can be used to improve volatile selectivity, which is achieved in PTR-TOF-MS normally by switching reagent ions [30].

Fig. 1 provides information on the measured and simulated percentages of the three reagent ions (including water clusters) determined using the total ion mode mentioned above, namely Fig. 1 (a) for $H_3O^+(H_2O)_n$, (b) for $NO^+(H_2O)_m$, and (c) for $O_2^{+\bullet}$ as a function of *E/N* and when using purified air with a volume-mixing ratio of H_2O ~ 100 ppm_v as the buffer gas in both the reaction and drift regions of the HiKE-IMS. For the simulations a water volume-mixing ratio was set to exactly 100 ppm_v. The simulations show that the reagent ion signal intensities for $NO^+(H_2O)_m$, $H_3O^+(H_2O)_n$, and $O_2^{+\bullet}$ are very sensitive to the value of the water concentration used. This is illustrated in Fig. 2 for simulated ion intensities using H_2O at concentration values corresponding to volume-mixing ratios of 50 ppm_v (left side of figure) and 150 ppm_v (right side of figure). Using H_2O volume-mixing ratios of 50 ppm_v and 150 ppm_v compared to the experimental value of ~ 100 ppm_v, it can be seen from these reagent ion simulations that there is a poorer agreement to the experimental values than that obtained in the simulation using an H_2O volume-mixing ratio of 100 ppm_v. This is particularly true for the $NO^+(H_2O)_m$ and $O_2^{+\bullet}$ signal intensities. The comparison of all simulated reagent ion intensities to the experimental values for the $H_3O^+(H_2O)_n$ reagent ions is discussed later.

In order to understand why $NO^+(H_2O)_m$ and $O_2^{+\bullet}$ remain as reagent ions in the HiKE-IMS, and not in a standard atmospheric pressure IMS system, and to explain their intensity dependences on *E/N* (effectively their dependence on reaction (drift) times and collisional energy), the ion chemistry and collisional induced processes that are occurring within the reaction and drift regions of the HiKE-IMS need to be considered. Although this has been discussed to some extent by Allers *et al* [26], here we provide more details on these processes and combine them with DFT calculations to provide the associated changes in enthalpy and free energy in order to have a firmer knowledge on the thermochemistry of the various ion reaction processes. Perhaps the most interesting observation is the dramatic increase in the percentage of the $O_2^{+\bullet}$ reagent ions with increasing *E/N*, which at first glance may seem strange, and hence we shall start with this.

3.1.1. Formation and loss of the $O_2^{+\bullet}$ reagent ions

The observed increase in intensity of $O_2^{+\bullet}$ with increasing *E/N* can be explained by the corresponding decrease in the associated reaction times and the decreasing water clustering owing to the higher collisional energies involved leading to rapid declustering. The results shown in Fig. 1(c) suggest that for low *E/N* (<50 Td) there is sufficient reaction time and limited collisional induced dissociation for the production of $O_2^{+\bullet}(H_2O)$ that can lead to a reaction sequence resulting in the production of hydronium ions and hence the complete removal of $O_2^{+\bullet}$ containing ions from the reaction region. Ion-molecule reaction mechanisms that are based on those proposed in the 1960s and 1970s for lower atmospheric chemistry can be adopted here to explain our observations [31–35], which have been also adopted for use in the paper by Allers *et al* [26].

Following production of $O_2^{+\bullet}$ in the HiKE-IMS ionisation source, via direct electron impact ionisation of O_2 through an electrical discharge in the corona source, or through a charge transfer reaction with $N_2^{+\bullet}$ [36], which itself is created through an electrical discharge that ionizes N_2, the initial process involves the formation of $O_2^{+\bullet}(H_2O)_p$ (p = 1 and 2) via the following association processes:

$$O_2^{+\bullet} + H_2O \rightarrow O_2^{+\bullet}(H_2O)\ \Delta H = -181\ kJ\ mol^{-1}\ \Delta G = -149\ kJ\ mol^{-1}, \quad (1)$$

and

$$O_2^{+\bullet}(H_2O) + H_2O \rightarrow O_2^{+\bullet}(H_2O)_2\ \Delta H = -106\ kJ\ mol^{-1}\ \Delta G = -72\ kJ\ mol^{-1}. \quad (2)$$

Following formation of $O_2^{+\bullet}(H_2O)$, and according to Fehsenfeld *et al* [31], a follow-on reaction with H_2O leads to the product ion $H_3O^+(OH^\bullet)$ via a fast exchange reaction at a rate coefficient of

$k = 1.9 \times 10^{-9}$ cm^3 s^{-1}, which is close to the collisional value:

$$O_2^{+\bullet}(H_2O) + H_2O \rightarrow H_3O^+(OH^\bullet) + O_2 \; \Delta H = -43 \text{ kJ mol}^{-1} \; \Delta G = -44 \text{ kJ mol}^{-1}. \quad (3)$$

However, this pathway must first involve the formation of $O_2^{+\bullet}(H_2O)_2$, because this is the most favourable route, both thermodynamically and mechanistically, which sequentially makes an intramolecular rearrangement to the proposed bimolecular reaction pathway (3). Thus,

$$O_2^{+\bullet}(H_2O)_2 \rightarrow H_3O^+(OH^\bullet) + O_2 \; \Delta H = +65 \text{ kJ mol}^{-1} \; \Delta G = +28 \text{ kJ mol}^{-1}, \quad (4)$$

with the overall process of $O_2^{+\bullet} + 2(H_2O)$ leading to $H_3O^+ + OH^\bullet + O_2$ being exoergic, ΔH = -125 kJ mol^{-1} and ΔG = -125 kJmol^{-1}. $H_3O^+(OH^\bullet)$ can also be rapidly converted to $H_3O^+(H_2O)$ via a switching reaction involving the replacement of $OH^\bullet$ with H_2O:

$$H_3O^+(OH^\bullet) + H_2O \rightarrow H_3O^+(H_2O) + OH^\bullet \; \Delta H = -59 \text{ kJ mol}^{-1} \; \Delta G = -55 \text{ kJ mol}^{-1}. \quad (5)$$

The amount of conversion of $O_2^{+\bullet}$ to $H_3O^+(OH^\bullet)$, and hence ultimately to $H_3O^+(H_2O)$, for fixed humidity, will be dependent on the reaction times and collisional energies as defined by *E/N*. Hence, with continuously increasing *E/N*, the ever decreasing reaction time and increasing collisional energy lead to a continuing reduction in the conversion of the $O_2^{+\bullet}$ ions to protonated water clusters, so that within the HiKE-IMS system $O_2^{+\bullet}$ becomes the dominant reagent ion species after about an *E/N* value of 80 Td under normal operating conditions. Given the high amount of oxygen in the system, $O_2^{+\bullet}$ will also be associating with O_2 to form $O_4^{+\bullet}$, and then a substitution reaction with water can lead to $O_2^{+\bullet}(H_2O) + O_2$, i.e., $O_4^{+\bullet}$ will also be lost through deionization, which ultimately leads to the production of protonated water clusters. Moreover, $O_2^{+\bullet}$ can also react via a bimolecular process with O_2 via resonant charge transfer. This has important implications for the ion mobility of $O_2^{+\bullet}$ in the drift region of the HiKE-IMS when operating in air. This is discussed later in section 3.4, which deals with the ion mobility spectra.

3.1.2. Formation and loss of the $H_3O^+(H_2O)_n$ (n = 0, 1, 2 and 3) reagent ions

Formation of $H_3O^+(H_2O)_n$ (with n = 0, 1, 2 and 3 for the experimentally observed ions found in this study) also takes place through the same reaction processes as occurs in atmospheric pressure IMS systems − namely sequential clustering, with the distribution of the $H_3O^+(H_2O)_n$ clusters being dependent on the humidity, gas temperature, and the type of buffer gas, and in the case of HiKE-IMS the value of the *E/N* within the drift tube. H_3O^+ is a short lived intermediate in atmospheric pressure IMS systems, and therefore the dominant reagent ions are $H_3O^+(H_2O)_n$ (n > 1). However, given the much higher values of *E/N* that are operating in the HiKE-IMS system, collision-induced dissociation of these ions results in rapid declustering (loss) and hence sufficient H_3O^+ ion intensities that increase with increasing *E/N*. Under the HiKE-IMS operational conditions used in this study with low humidity air (~ 100 ppm$_v$) (normal operating conditions), the mass spectral analysis indicates that H_3O^+ appears to have become the dominant water containing reagent ion available for reaction above approximately 90 Td, although at somewhat lower concentrations than that found for $O_2^{+\bullet}$. However, compared to the simulations, the experimental mass spectrometric values indicate that far less water clustering is observed to occur than should be expected (see Fig. 1). In the simulations, even protonated water clusters up to n = 4 (although in small amounts) are found. However, the simulations do not reflect any possible collisional induced processes that occur in the transfer region between the end of the drift tube of the HiKE-IMS and the TOF-MS, as discussed by Allers *et al* [22]. If this occurs, as is suggested from a comparison of the simulated to experimental reagent ion percentages, there is no reason to expect a simple one-to-one correspondence between what is detected at the micro channel plate of the TOF-MS and the actual protonated water cluster distribution that is present in the drift tube of the HiKE-IMS for a fixed *E/N* value. Thus, the simulations may provide more realistic information on what is actually present for the protonated water cluster distributions in the drift tube of the HiKE-IMS than the experimental mass spectrometric values provide. However, given the simplicity of the simulations, they can only provide semi-quantitative information at best. Furthermore, the simulations cannot be a completely accurate representation of what is present, because other studies have shown that there must be significant H_3O^+ available for reaction in the HiKE-IMS for *E/N* above about 90 Td, even when the reaction region is under high humidity conditions [37].

3.1.3. $NO^+(H_2O)_m$ (m = 0 and 1) reagent ions

Unlike $O_2^{+\bullet}$ and $H_3O^+(H_2O)_n$, the NO^+ reagent ions do not demonstrate a strong dependence on *E/N*, only $NO^+(H_2O)$ shows any dependence. This is largely due to the fact that to convert NO^+ to the terminal protonated water clusters, $NO(H_2O)_3^+$ needs to be formed [35]. Here we propose that initially third body association occurs:

$$NO^+ + H_2O \rightarrow NO^+(H_2O) \; \Delta H = -118 \text{ kJmol}^{-1} \; \Delta G = -88 \text{ kJ mol}^{-1} \quad (6)$$

and

$$NO^+(H_2O) + H_2O \rightarrow NO^+(H_2O)_2 \; \Delta H = -84 \text{ kJmol}^{-1} \; \Delta G = -45 \text{ kJ mol}^{-1}. \quad (7)$$

Intramolecular rearrangement of $NO^+(H_2O)_2$ via a transition state leading to $H_3O^+(HONO)$ is calculated to be endoergic:

$$NO^+(H_2O)_2 \rightarrow H_3O^+(HONO) \; \Delta H = +78 \text{ kJ mol}^{-1} \; \Delta G = +86 \text{ kJ mol}^{-1}. \quad (8)$$

However, following a third association, intramolecular rearrangement leading to a reagent ion not containing NO then becomes thermoneutral:

$$NO^+(H_2O)_3 \rightarrow H_3O^+(H_2O) + HNO_2 \; \Delta H = -6 \text{ kJmol}^{-1} \; \Delta G = -1 \text{ kJ mol}^{-1}. \quad (9)$$

Given that the NO^+ signal intensities (percentages) remain stable throughout the *E/N* range investigated, we can safely assume from the experimental and simulated results presented in Fig. 1(b) that only a small contribution to the $H_3O^+(H_2O)$ signal occurs via pathway (9), and then only at very low *E/N* (<40 Td).

3.2. Reagent ion distribution as a function of E/N using humidified sample air (at inlet an H_2O volume-mixing ratio of ~4000 ppm$_v$) and "normal" (low humidity) drift air (H_2O volume-mixing ratio of ~100 ppm$_v$)

Fig. 3 provides information on the measured and simulated percentages of the reagent ions as a function of *E/N* over the range of 30−115 Td. This shows a dramatic change in ion signal intensities compared to the lower humidity (~ 100 ppm$_v$) measurements presented in Fig. 1. Instead of three, only two types of reagent ions

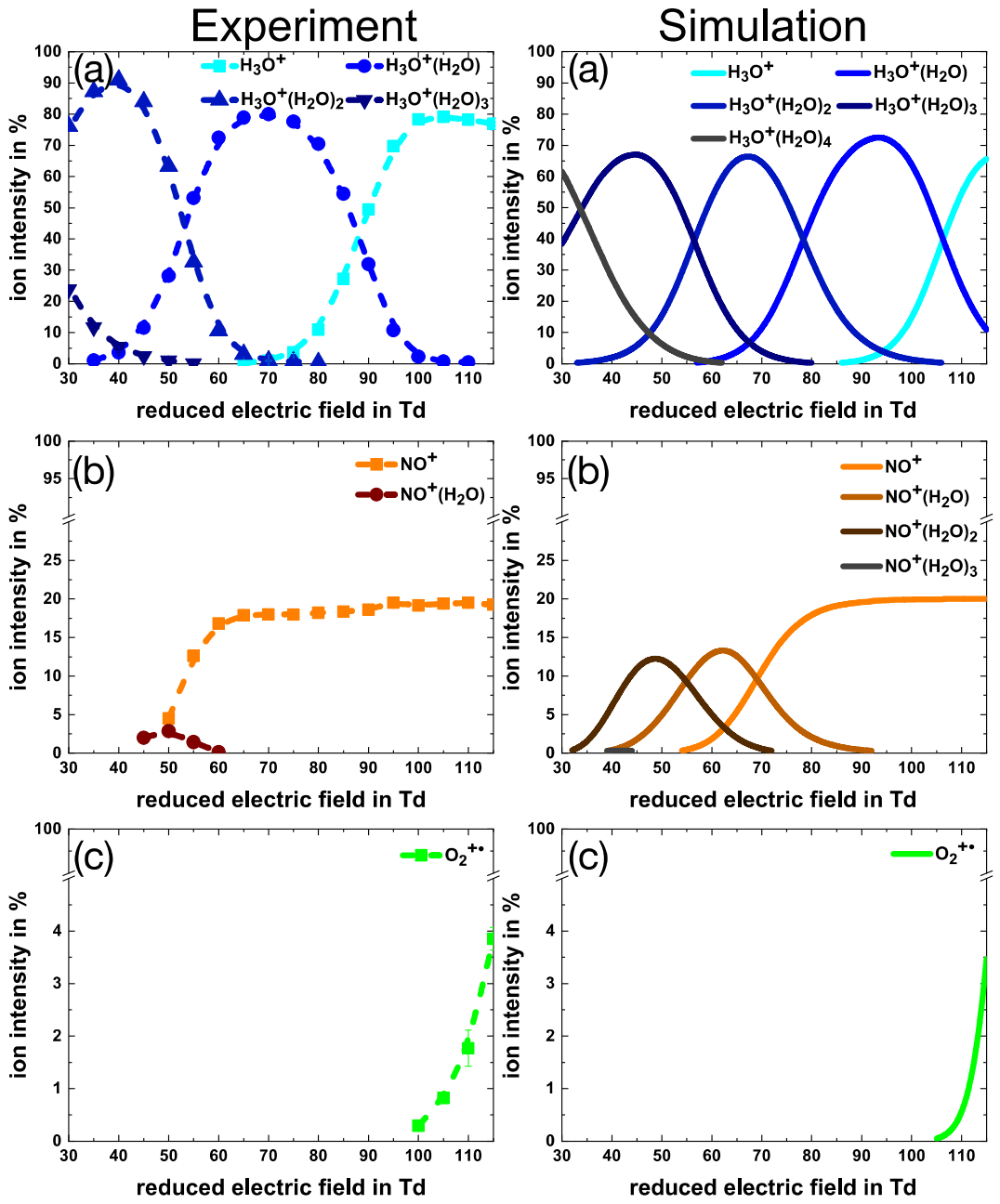

Fig. 3. HiKE-IMS-TOF-MS positive reagent ion percentage distributions (measured and simulated) using humidified (~ 4000 ppm_v) sample and dry drift (~ 100 ppm_v) inlet air flows as a function of *E/N*. For clarity, the three types of reagent ions, namely (a) $H_3O^+(H_2O)_n$, (b) $NO^+(H_2O)_m$, and (c) $O_2^{+\bullet}$ are shown separately. To determine the experimental percentages, no allowance has been made for any *m/z* transmission dependencies. An H_2O volume-mixing ratio of 1555 ppm_v simulated the best $O_2^{+\bullet}$ signal in comparison to the experimental measurements.

are now experimentally found to be dominant, namely $H_3O^+(H_2O)_n$ (n = 0, 1, 2 and 3) and $NO^+(H_2O)_m$ (m = 0 and 1). It can be seen that the $O_2^{+\bullet}$ signal is significantly suppressed compared to that for which both the sample and drift gas flows are under relatively dry (~ 100 ppm_v) conditions. This is because at the higher humidity in the reaction region the formation of $O_2^{+\bullet}(H_2O)$ and $O_2^{+\bullet}(H_2O)_2$ ions is favoured over the full range of *E/N*, which in turn react with water to form ultimately the $H_3O^+(H_2O)_n$ terminal reagent ions before entry to the drift region. To obtain a good qualitative agreement with the experimental observation, a water volume-mixing ratio value of 1555 ppm_v had to be set for the simulations, which is less than that measured entering from the reaction region (~ 4000 ppm_v). However, it needs to be appreciated that only relatively low humid air is used as the drift gas, which will lower the volume-mixing ratio in the reaction region. In agreement with this, a water volume-mixing ratio is measured to be ~ 2000 ppm_v in the exhaust line.

3.3. *Product ion distribution as a function of E/N for "normal" (low humidity) air (H_2O volume-mixing ratio of ~100 ppm_v) for both sample and drift gas flows*

Fig. 4 shows the product ions detected under normal operating conditions (H_2O ~ 100 ppm_v) as a function of *E/N*. As described above, these product ions predominantly result from reactions with $O_2^{+\bullet}$, but also to some extent H_3O^+. Based on the ionisation energy

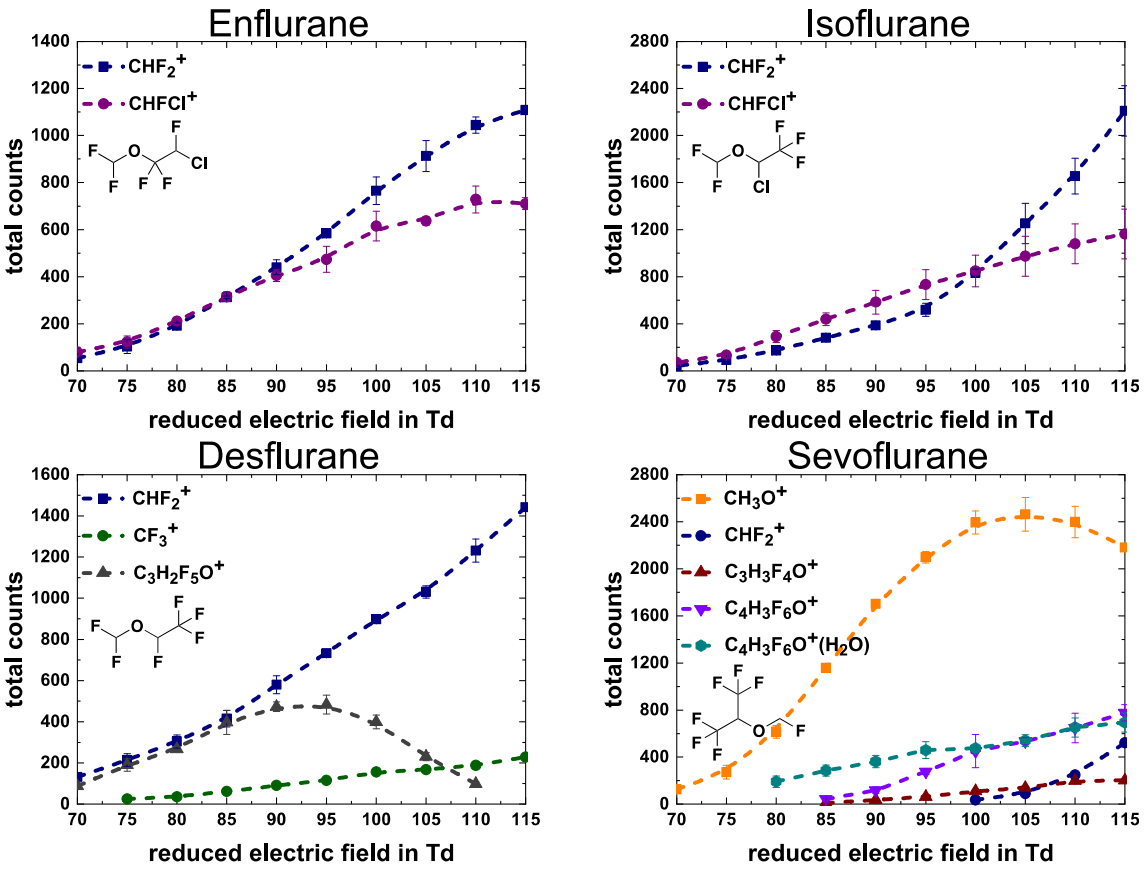

Fig. 4. Product ion signals (total counts over a 90 s integration time) for the enflurane, isoflurane, desflurane, and sevoflurane in purified dry air (sample and drift gas at ~ 100 ppm_v) as a function of *E/N*. Measurements for each *E/N* value were taken three times and the associated standard deviation is shown as error bars.

of enflurane at 11.7–12.2 eV [38], and the fact that the RIP associated with the NO^+ containing reagent ions does not show any decrease in intensity when the fluranes are introduced into the reaction region (see Fig. 5) we can exclude electron transfer to the NO^+ containing reagent ions from any of the four fluranes. This is in line with the low recombination energy of NO^+ (9.26 eV). NO^+ could potentially react via a three body process with the fluranes to form adducts, as has been observed in a SIFT-MS study with isoflurane ($NO^+.C_3H_2ClF_5O$) and seveoflurane ($NO^+.C_4H_3F_7O$) [18], but SIFT-MS studies are undertaken under thermal (300 K) conditions, i.e., collisional induced dissociation would not have occurred in the flow tube of the instrument. Given the higher non-thermal

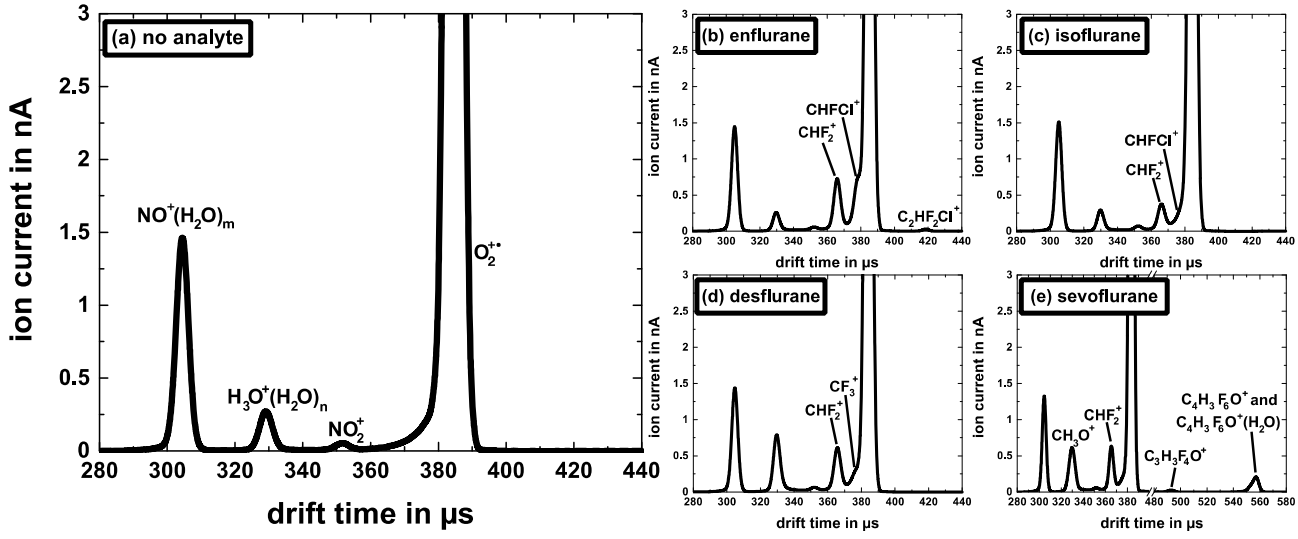

Fig. 5. HiKE-IMS ion mobility spectra recorded under normal operating airflow conditions (H_2O volume-mixing ratio ~ 100 ppm_v) used for both sample and drift airflows at an *E/N* of 115 Td containing (a) no analyte and with (b) enflurane, (c) isoflurane, (d) desflurane and (e) sevoflurane having been introduced into the reaction region in trace amounts.

collisional energies involved in the HiKE-IMS, no adduct ion, even if formed, is likely to survive in the reaction or drift regions. Indeed none is observed in the mass spectra, unless of course they fragment in the ion transfer region, which cannot be completely ruled out, especially at low *E/N* values.

For the two isomers, enflurane and isoflurane, two product ions have been identified in the mass spectra at *m/z* 51 (CHF_2^+) and *m/z* 67/69 ($CHFCl^+$). For enflurane, two other *m/z* peaks were observed in the mass spectra, at approximately *m/z* 98 and *m/z* 100. However, their associated intensities were extremely low, which made definitive *m/z* assignment and hence product ion identification difficult. Therefore, we investigated the reactions of enflurane (and all the other fluranes) with $O_2^{+\bullet}$ using a high sensitive (> 2000 cps/ppbv, with a detection limit < 1 ppt_v (in 60 s)) and high mass resolution (>6000 $m/\Delta m$ (FWHM)) PTR-TOF-MS, namely an Ionicon Analytik GmbH PTR-TOF 6000 × 2 [39]. The full results of that study will be the subject of another paper. Here we just confirm that two spectral peaks (among others) in the mass spectrum that results from the reaction of $O_2^{+\bullet}$ with enflurane are observed at *m/z* 97.97 and 99.97, with their relative intensities in the ratio of approximately 3 to 1, respectively, which is consistent with the corresponding product ion containing one chlorine atom. Given this, and that the measured *m/z* peak positions are at a high accuracy, we can state that the product ion that produces low intensity signals at about *m/z* 98 and *m/z* 100 in the HiKE-IMS-MS measurements result from $C_2HF_2Cl^+$. Three product ions are observed for desflurane at *m/z* 51 (CHF_2^+), *m/z* 69 (CF_3^+), and *m/z* 149 ($C_3H_2F_5O^+$). For sevoflurane, product ions were observed at *m/z* values of 31, 51, 131, 181 and 199, which are assigned to be the product ions CH_3O^+, CHF_2^+, $C_3H_3F_4O^+$, $C_4H_3F_6O^+$, and $C_4H_3F_6O^+(H_2O)$, respectively. For the last two sevoflurane product ions, i.e., $C_4H_3F_6O^+$ and $C_4H_3F_6O^+(H_2O)$, interconversion down the drift region must occur because of their identical drift times. For convenience, Table 1 provides a summary of the relative intensities of the product ions for three sample *E/N* values, namely 80, 100 and 115 Td.

Similar product ions to those observed in this study have been reported from the PTR-TOF-MS and SIFT-MS studies [14,17,18]. A direct quantitative comparison of the product ions between the three analytical instruments is not useful owing to the presence of the two reagent ions that react with the fluranes in the reaction region of the HiKE-IMS and because of differences in sensitivities for ion detection between the instruments. It is sufficient that good qualitative agreement has been obtained between all soft chemical ionisation mass spectrometric and HiKE-IMS measurements. However, we comment on one particular anomaly, that is of CH_2FO^+ (*m/z* 49) being a significant product ion observed in the two SIFT-MS studies of sevoflurane [17,18], but not in this HiKE-IMS study or in our earlier PTR-TOF-MS investigation [14]. The study by Wang *et al* [18] showed that this product ion results from reactions with both H_3O^+ and $O_2^{+\bullet}$, with its intensity increasing with increasing reaction length, which indicates that, in part, this could also be a result of a secondary reaction. Thus, there are interesting complications associated with the ion-chemistry of these fluranes that need further investigation. This is further emphasised by the additional observation of Wang *et al* that H_3O^+/sevoflurane ion chemistry catalyses the production of H_3O^+.

According to the DFT calculated proton affinities (PAs) and gas phase basicities (GBs) provided in the paper by Malásková *et al* [14], the four fluranes cannot react with protonated water clusters via proton transfer. This is evident by comparing the calculated PA (H_2O) = 684 $kJmol^{-1}$ and GB (H_2O) = 653 $kJmol^{-1}$ and PA $(H_2O)_2$ = 842 $kJmol^{-1}$ and GB $(H_2O)_2$ = 777 $kJmol^{-1}$ with the calculated PA (desflurane) = 652 kJ mol^{-1} and GB (desflurane) = 638 kJ mol^{-1}, PA (sevoflurane) = 678 kJ mol^{-1} and GB (sevoflurane) = 660 kJ mol^{-1}, PA (isoflurane) = 670 kJ mol^{-1} and GB (isoflurane) = 665 kJ mol^{-1}, and PA (enflurane) = 662 kJ mol^{-1} and GB (enflurane) = 646 kJ mol^{-1} (with the PA and GB values given for the fluranes corresponding to the most energetically favoured protonation sites). Thus, proton transfer from H_3O^+ is close to being thermoneutral for sevoflurane (ΔG_{298} = -7 kJ mol^{-1}) and isoflurane (ΔG_{298} = -2 kJ mol^{-1}), and can be driven by the collisional energy gained in the electric field for enflurane and desflurane, and following this proton transfer dissociation in the product ions rapidly occurs [14]. Proton transfer reactions with the protonated water clusters are highly endoergic, and therefore cannot take place. Moreover, as discussed above, and from the SIFT-MS study of Wang *et al* [18], $O_2^{+\bullet}$ has sufficient recombination energy (12.07 eV) to react with all the fluranes via dissociative charge transfer.

3.4. Reagent and product ions mobility spectra in the HiKE-IMS under conditions of low humidity

Fig. 5 presents examples of the HiKE-IMS ion mobility spectra using "normal" air in the drift tube (with an H_2O volume-mixing ratio of ~ 100 ppmv) for (a) reagent ions with no analyte present (the RIPs) and the reagent and product ions for (b) enflurane, (c)

Table 1
Product ion intensities in percentages at three *E/N* values of 80, 100, and 115 Td with air as the buffer gas with a water volume-mixing ratio of ~ 100 ppm_v. The molecular formula for the product ions are given, together with their nominal *m/z* values for the main isotopologues. Errors on percentages are conservatively estimated to be of the order of ±10%.

Analyte,sum formula, monoisotopic-mass	Product Ions nominal (*m/z*)	Product Ion Intensities in %		
		80 Td	100 Td	115 Td
enflurane	CHF_2^+ (51)	48	56	62
$C_3H_2ClF_5O$	$CHFCl^+$ (67/69)	52	44	38
183.97 g mol^{-1}				
isoflurane	CHF_2^+ (51)	38	48	65
$C_3H_2ClF_5O$	$CHFCl^+$ (67/69)	62	52	35
183.97 g mol^{-1}				
desflurane	CHF_2^+ (51)	50	62	86
$C_3H_2F_6O$	CF_3^+ (69)	6	11	14
168.00 g mol^{-1}	$C_3H_2F_5O^+$ (149)	44	27	–
sevoflurane	CH_3O^+ (31)	77	69	50
$C_4H_3F_7O$	CHF_2^+ (51)	–	1	12
200.01 g mol^{-1}	$C_3H_3F_4O^+$ (131)	–	3	4
	$C_4H_3F_6O^+$ (181)	–	13	18
	$C_4H_3F_6O^+(H_2O)$ (199)	23	14	16

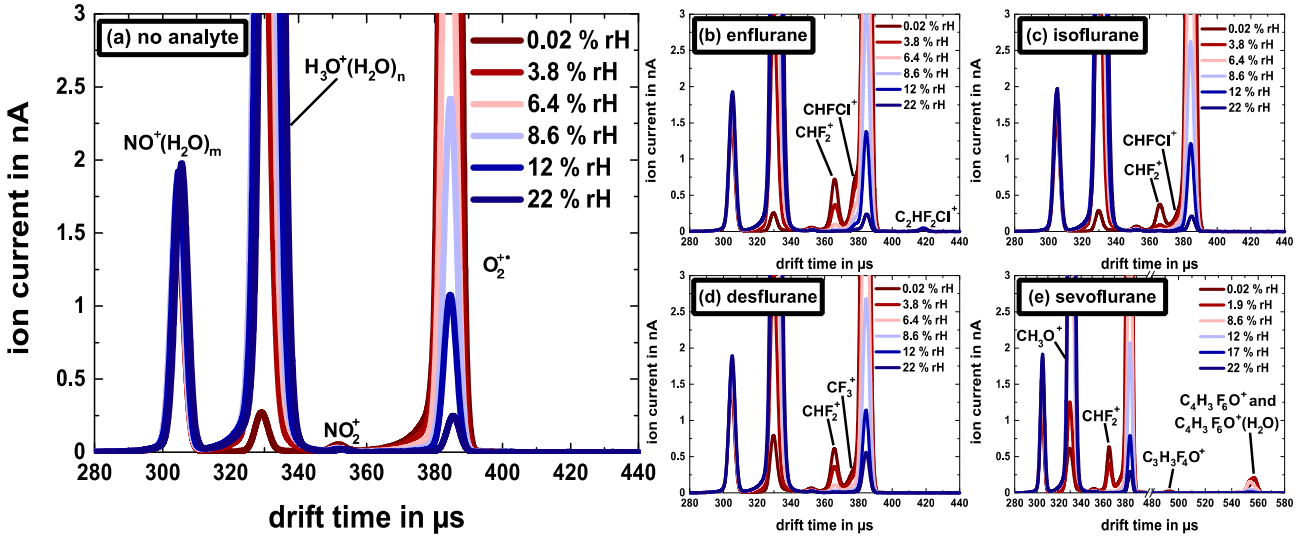

Fig. 6. HiKE-IMS ion mobility spectra for different inlet relative humidity (rH) sample airflows whilst maintaining the inlet drift air at ~ 100 ppm_v for (a) no analyte (the RIPs), (b) enflurane, (c) isoflurane, (d) desflurane and (e) sevoflurane. The drift airflow was maintained at ~ 100 ppm_v. All of the ion mobility spectra shown were recorded at an *E/N* of 120 Td.

isoflurane, (d) desflurane and (e) sevoflurane. The ion mobility spectra were all recorded at the same fixed *E/N* value of 115 Td.

In Fig. 5 (a) (no analyte), three RIPs can be identified. These are, in order of their increasing drift times, $NO^+(H_2O)_m$, $H_3O^+(H_2O)_n$ and $O_2^{+\bullet}$. Comparing the reagent ion drift times with the product ions for the four fluranes, it can be seen that the drift times for certain product ions with $m/z > 32$ are less than that found for $O_2^{+\bullet}$. These include CHF_2^+ and $CHFCl^+$ for isoflurane and enflurane, CHF_2^+ and CF_3^+ for desflurane, and CH_3O^+ and CHF_2^+ for sevoflurane. That all of these product ions have lower drift times than that of $O_2^{+\bullet}$ in the HiKE-IMS, is perhaps not what should be expected, especially given that the drift times for the product ion CH_3O^+ associated with sevoflurane, which has an m/z close to that of $O_2^{+\bullet}$, is clearly much shorter than that of $O_2^{+\bullet}$. However, the long drift times associated with $O_2^{+\bullet}$ can be explained by the phenomenon of resonant charge transfer: $O_2^{+\bullet} + O_2 \rightleftharpoons O_2^{+\bullet}.O_2 \rightleftharpoons O_2 + O_2^{+\bullet}$ in the drift region [22]. Following charge transfer, the new $O_2^{+\bullet}$ will start with essentially a zero mean velocity in the direction of the Faraday plate. Acceleration in the electric field and decelerations through collisions will ultimately result in this $O_2^{+\bullet}$ attaining a drift velocity appropriate to that of $O_2^{+\bullet}$, but this will take time. Then another resonant charge transfer occurs, starting the process all over again. This "stopping", which is caused by the resonant charge transfer, and "starting" (initial acceleration by the *E* field, leading to a terminal speed through deceleration from collisions with the buffer gas) of the $O_2^{+\bullet}$ reagent ions in the drift tube results in the observed decrease in the mobility of $O_2^{+\bullet}$. This leads to $O_2^{+\bullet}$ having a significantly longer drift time in the drift tube than it would otherwise have if no oxygen were present [40]. A slightly alternative argument that could explain the longer drift times is that $O_2^{+\bullet}$ forms a loosely bound complex with O_2, and the charge is resonantly oscillating between the two oxygen molecules, so that effectively we are dealing with the transit of $O_4^{+\bullet}$, down the drift region, which results in the longer drift times observed than would be for $O_2^{+\bullet}$.

Possible evidence for the alternative argument comes, and as mentioned earlier, from $O_4^{+\bullet}$ being observed, although in low intensities in the mass spectrum. Its drift time is observed to be the same as that for $O_2^{+\bullet}$, which is to be expected if the majority of its formation is through the transient species $O_2^{+\bullet}.O_2$ leading to resonant charge transfer. The low ion intensity associated with $O_4^{+\bullet}$ is consistent with the transient nature of $O_2^{+\bullet}.O_2$ and possible fragmentation through collisional processes as it passes through the three grid construction at the end of the drift tube to the ion transfer optics region. Another route for $O_4^{+\bullet}$ production is through three-body association, which will also be susceptible to dissociation during its transfer from the drift tube of the HiKE-IMS into the TOF-MS. Given its low intensity, we have ignored it as a major contribution to the reagent ion-mobility peak assigned to $O_2^{+\bullet}$.

3.5. Product ion formation as a function of E/N using humidified air in the reaction region (inlet H_2O volume-mixing ratio ~4000 ppm_v)

For those investigations using higher humidity in the reaction region, no product ions were observed over an *E/N* range of 30–100 Td. Only very small product ion signal intensities were observed above about an *E/N* of 105 Td, presumably resulting from reactions with the remaining $O_2^{+\bullet}$, which itself is present in the reaction region only in low concentrations. Even at an *E/N* of 115 Td, $O_2^{+\bullet}$ accounts for only about 4% of the total reagent ion signal (see Fig. 3). Product ions observed are given as $CHFCl^+$ for enflurane and isoflurane, $C_4H_3F_6O^+$ for sevoflurane, and CHF_2^+ for desflurane.

Given the dramatic loss of reagent and product ion signals under the higher humid conditions, we have investigated the changes in product ion intensities as the humidity of the air entering the reaction region was changed from being relatively dry to about 25% rH. The drift airflow remained at an H_2O volume-mixing ratio of about 100 ppm_v.

The resulting ion mobility spectra as a function of sample inlet humidity are summarised in Fig. 6, all of which were recorded at an *E/N* value of 120 Td. From Fig. 6 it can be seen that with increasing humidity the $O_2^{+\bullet}$ and the analyte ion mobility peak intensities progressively decrease, whilst the one associated with $H_3O^+(H_2O)_n$ steadily increases. The $NO^+(H_2O)_m$ ion signals remain essentially unaltered. This is to be expected, the explanation for which has already been provided in the previous discussions above.

The continuing loss of product ion signal with increasing humidity in the reaction region could be taken to suggest that no H_3O^+ is present in the reaction region, with $H_3O^+(H_2O)_n$ (n = 1, 2, 3 …) becoming the dominant reagent ions. If that is the case, then a volatile, M, that has a proton affinity less than that of $(H_2O)_m$ (m > 1), or for which a substitution reaction is not energetically available, namely $H_3O^+(H_2O)_n + M \rightarrow MH^+(H_2O)_x + yH_2O$

(x + y = n+1), then the volatile cannot be detected with a good sensitivity. However, that cannot be the case for HiKE-IMS, for which there is evidence to suggest that H_3O^+ is present for reaction in the ionisation region. The loss or changes of product ion signal with increasing humidity is therefore not fully understood, but this behaviour has also been noted in the SIFT-MS and PTR-TOF-MS studies of Wang *et al* [18], and Malásková *et al* [14], respectively.

4. Concluding remarks

This paper has presented the first positive ion HiKE-IMS-MS studies of four fluranes, three of which are currently used as inhalation anaesthetics. The aim was to investigate the HiKE-IMS potential to detect in real-time the four fluorinated compounds in either low humidity air (e.g., in a room environment) or in humid air (i.e., relating to breath analysis) and compare that with similar measurements made with PTR-MS. These studies show that HiKE-IMS would be well suited for air quality control of these fluranes, e.g., in operating theatres, but that in humid air, and as found in PTR-MS studies, the sensitivity of the HiKE-IMS for detection of the four anaesthetics is too low to be of practical use for breath analysis. In part, this is because of the complex ion chemistry that occurs in the HiKE-IMS over all *E/N* values that significantly suppresses both $O_2^{+\bullet}$ and because of thermodynamically unfavourable substitution reactions with $H_3O^+(H_2O)_n$ ($n \geq 1$) [41]. However, there should still be sufficient H_3O^+ reagent ions in the reaction region for proton transfer to occur. One possible explanation is that once MH^+ is formed, there is a back reaction with H_2O leading to its loss before the transient product ion has a chance to dissociate. However, if that were to occur, it would also have happened under the high humid conditions used in the PTR-TOF-MS measurements of Malásková *et al* [14]. One plausible explanation is that the product ions formed are lost through secondary reactions with water.

An interesting observation, was the dependence of the $O_2^{+\bullet}$ intensity on *E/N*, as shown in Fig. 1(c). This has been carefully explained in section 3.1.1. However, it raises the question as to why $O_2^{+\bullet}$ is not a major reagent ion in PTR-MS instruments when using water to generate reagent ions and operating in air? The answer to this must relate in part to the design of the ion source being used. Within the ionisation source and transfer region to the drift tube (the reaction region) of a PTR-MS, there must be sufficient reaction time and reactions to eliminate the majority of $O_2^{+\bullet}$ (and NO^+) containing precursor ions, leading to less complex ion chemistry in the reaction drift tube region compared to that occurring in a HiKE-IMS. This implies that if a different ionisation source in a HiKE-IMS were to be used, namely something that is closer to that used in a PTR-MS, then this should result in $H_3O^+(H_2O)_n$ reagent ions becoming the dominant species in the reaction region over a large range of *E/N*, just as occurs in the higher pressure standard IMS system, for which only one reagent ion peak is observed, but for HiKE-IMS under much lower drift tube pressures. Investigations and development of different HiKE-IMS ion sources will be the subject of further study.

Although operating the HiKE-IMS in positive ion mode highlighted challenges for detecting the fluranes in humid air, which is of relevance to breath analysis, the fluranes should be readily detected in breath with high sensitivity by operating the HiKE-IMS in negative ion mode, as demonstrated in a number of recent negative ion IMS studies [42,43]. This will also be the subject of a separate investigation.

For the continuing development of HiKE-IMS as an analytical tool, this study has highlighted the need to understand fully the ion-chemistry occurring in the reaction region of the HiKE-IMS for analytes of analytical interest; ion-chemistry bridging that operating in PTR-TOF-MS and atmospheric pressure IMS systems.

Author statement

Florentin Weiss: Investigation, Data Analysis, Visualization, Writing Original and Final Drafts.

Christoph Schaefer: Assisting in Investigation, Writing - Review & Editing.

Veronika Ruzsanyi: Writing - Review & Editing, Supervision, Project Administration

Tilmann Märk: Writing - Review & Editing.

Gary Eiceman: Writing - Review & Editing.

Chris A. Mayhew: Project Proposal, Writing Original and Final Drafts, Supervision

Stefan Zimmermann: Writing - Review & Editing.

Declaration of competing interest

The authors declare that they have no known competing financial interests or personal relationships that could have appeared to influence the work reported in this paper.

Acknowledgements

We wish to acknowledge the Austrian Research Promotion Agency (FFG) for the support of this study through the program KIRAS Security Research under the grant TRACK (grant agreement no. 24146100) and, in particular, for the funding of Florentin Weiss's PhD programme. Furthermore, we would like to acknowledge the Deutsche Forschungsgemeinschaft (DFG, German Research Foundation) for funding - 318063177 and 390583968.

References

[1] M. Loscar, P. Conzen, Volatile Anästhetika, Anaesthesist 53 (2004) 183–198, https://doi.org/10.1007/s00101-003-0632-6.
[2] B.A. Hitt, R.I. Mazze, M.J. Cousins, H.N. Edmunds, G.A. Barr, J.R. Trudell, Metabolism of isoflurane in Fischer 344 rats and man, Anesthesiology 40 (1974) 62–67, https://doi.org/10.1097/00000542-197401000-00015.
[3] M. Heck, Repetitorium anasthesiologie: Fur die facharztprufung und das europaische diplom, Springer, 2010 [Place of publication not identified].
[4] E.M. Sakai, L.A. Connolly, J.A. Klauck, Inhalation anesthesiology and volatile liquid anesthetics: focus on isoflurane, desflurane, and sevoflurane, Pharmacotherapy 25 (2005) 1773–1788, https://doi.org/10.1592/phco.2005.25.12.1773.
[5] C. Ager, P. Mochalski, J. King, C.A. Mayhew, K. Unterkofler, Effect of inhaled acetone concentrations on exhaled breath acetone concentrations at rest and during exercise, J. Breath Res. 14 (2020) 26010, https://doi.org/10.1088/1752-7163/ab613a.
[6] L. La Colla, A. Albertin, G. La Colla, A. Mangano, Faster wash-out and recovery for desflurane vs sevoflurane in morbidly obese patients when no premedication is used, Br. J. Anaesth. 99 (2007) 353–358, https://doi.org/10.1093/bja/aem197.
[7] R.J. Gardner, Inhalation anaesthetics–exposure and control: a statistical comparison of personal exposures in operating theatres with and without anaesthetic gas scavenging, Ann. Occup. Hyg. 33 (1989) 159–173, https://doi.org/10.1093/annhyg/33.2.159.
[8] J. Rieder, P. Prazeller, M. Boehler, P. Lirk, W. Lindinger, A. Amann, Online monitoring of air quality at the postanesthetic care unit by proton-transfer-reaction mass spectrometry, Anesth. Analg. 92 (2001) 389–392, https://doi.org/10.1097/00000539-200102000-00021.
[9] J. Rieder, C. Keller, J. Brimacombe, G. Gruber, P. Lirk, G. Summer, A. Amann, Monitoring pollution by proton-transfer-reaction mass spectrometry during paediatric anaesthesia with positive pressure ventilation via the laryngeal mask airway or uncuffed tracheal tube, Anaesthesia 57 (2002) 663–666, https://doi.org/10.1046/j.1365-2044.2002.02622.x.
[10] G. Summer, P. Lirk, K. Hoerauf, U. Riccabona, F. Bodrogi, H. Raifer, M. Deibl, J. Rieder, W. Schobersberger, Sevoflurane in exhaled air of operating room personnel, Anesth. Analg. 97 (2003) 1070–1073, https://doi.org/10.1213/01.ANE.0000081796.67539.27, table of contents.
[11] G.R. Harrison, A.D.J. Critchley, C.A. Mayhew, J.M. Thompson, Real-time breath monitoring of propofol and its volatile metabolites during surgery using a novel mass spectrometric technique: a feasibility study, Br. J. Anaesth. 91 (2003) 797–799, https://doi.org/10.1093/bja/aeg271.
[12] P. Lirk, F. Bodrogi, J. Rieder, Medical applications of proton transfer reaction-mass spectrometry: ambient air monitoring and breath analysis, Int. J. Mass Spectrom. 239 (2004) 221–226, https://doi.org/10.1016/j.ijms.2004.07.016.

[13] Philipp Sulzer, Alfons Jordan, Märk Lukas, Christopher A. Mayhew, Kurt Becker, Tilmann D. Märk, Technical advances in proton transfer reaction-mass spectrometry and new fields of application, Am. Lab. 43 (2011) 13–15.
[14] M. Malásková, D. Olivenza-León, P.D. Chellayah, J. Martini, W. Lederer, V. Ruzsanyi, K. Unterkofler, P. Mochalski, T.D. Märk, P. Watts, C.A. Mayhew, Studies pertaining to the monitoring of volatile halogenated anaesthetics in breath by proton transfer reaction mass spectrometry, J. Breath Res. 14 (2020) 26004, https://doi.org/10.1088/1752-7163/ab5e30.
[15] A. Hansel, A. Jordan, R. Holzinger, P. Prazeller, W. Vogel, W. Lindinger, Proton transfer reaction mass spectrometry: on-line trace gas analysis at the ppb level, Int. J. Mass Spectrom. Ion Process. 149-150 (1995) 609–619, https://doi.org/10.1016/0168-1176(95)04294-U.
[16] A.M. Ellis, C.A. Mayhew, Proton Transfer Reaction Mass Spectrometry: Principles and Applications, John Wiley & Sons, Inc, Chichester, West Sussex, UK, 2014.
[17] A. Critchley, T.S. Elliott, G. Harrison, C.A. Mayhew, J.M. Thompson, T. Worthington, The proton transfer reaction mass spectrometer and its use in medical science: applications to drug assays and the monitoring of bacteria, Int. J. Mass Spectrom. 239 (2004) 235–241, https://doi.org/10.1016/j.ijms.2004.08.008.
[18] T. Wang, D. Smith, P. Spaněl, Selected ion flow tube studies of the reactions of H3O+, NO+ and O2+ with the anaesthetic gases halothane, isoflurane and sevoflurane, Rapid Commun. Mass Spectrom. 16 (2002) 1860–1870, https://doi.org/10.1002/rcm.804.
[19] A. Ahrens, S. Zimmermann, Towards a hand-held, fast, and sensitive gas chromatograph-ion mobility spectrometer for detecting volatile compounds, Anal. Bioanal. Chem. 413 (2021) 1009–1016, https://doi.org/10.1007/s00216-020-03059-9.
[20] J. Langejuergen, M. Allers, J. Oermann, A. Kirk, S. Zimmermann, High kinetic energy ion mobility spectrometer: quantitative analysis of gas mixtures with ion mobility spectrometry, Anal. Chem. 86 (2014) 7023–7032, https://doi.org/10.1021/ac5011662.
[21] M. Allers, A.T. Kirk, N. von Roßbitzky, D. Erdogdu, R. Hillen, W. Wissdorf, T. Benter, S. Zimmermann, Analyzing positive reactant ions in high kinetic energy ion mobility spectrometry (HiKE-IMS) by HiKE-IMS-MS, J. Am. Soc. Mass Spectrom. 31 (2020) 812–821, https://doi.org/10.1021/jasms.9b00087.
[22] M. Allers, A.T. Kirk, C. Schaefer, D. Erdogdu, W. Wissdorf, T. Benter, S. Zimmermann, Field-dependent reduced ion mobilities of positive and negative ions in air and nitrogen in high kinetic energy ion mobility spectrometry (HiKE-IMS), J. Am. Soc. Mass Spectrom. 31 (2020) 2191–2201, https://doi.org/10.1021/jasms.0c00280.
[23] A. Good, D.A. Durden, P. Kebarle, Mechanism and rate constants of ion–molecule reactions leading to formation of H + (H 2 O) n in moist oxygen and air, J. Chem. Phys. 52 (1970) 222–229, https://doi.org/10.1063/1.1672668.
[24] Y.K. Lau, S. Ikuta, P. Kebarle, Thermodynamics and kinetics of the gas-phase reactions H3O+(H2O)n-1 + water = H3O+(H2O)n, J. Am. Chem. Soc. 104 (1982) 1462–1469, https://doi.org/10.1021/ja00370a002.
[25] A.T. Kirk, D. Grube, T. Kobelt, C. Wendt, S. Zimmermann, High-resolution high kinetic energy ion mobility spectrometer based on a low-discrimination tristate ion shutter, Anal. Chem. 90 (2018) 5603–5611, https://doi.org/10.1021/acs.analchem.7b04586.
[26] M. Allers, A.T. Kirk, M. Eckermann, C. Schaefer, D. Erdogdu, W. Wissdorf, T. Benter, S. Zimmermann, Positive reactant ion formation in high kinetic energy ion mobility spectrometry (HiKE-IMS), J. Am. Soc. Mass Spectrom. 31 (2020) 1291–1301, https://doi.org/10.1021/jasms.0c00114.
[27] P.W. Atkins, J. de Paula, J. Keeler, Atkins' Physical Chemistry, eleventh ed., Oxford University Press, Oxford, New York, 2018.
[28] G.H. Wannier, Motion of gaseous ions in strong electric fields, Bell Syst. Tech. J. 32 (1953) 170–254, https://doi.org/10.1002/j.1538-7305.1953.tb01426.x.
[29] M.J. Frisch, et al., Gaussian 09 Revision A.1, CT: Gaussian, Inc., Wallingford, 2009.
[30] P. Sulzer, B. Agarwal, S. Jürschik, M. Lanza, A. Jordan, E. Hartungen, G. Hanel, L. Märk, T.D. Märk, R. González-Méndez, P. Watts, C.A. Mayhew, Applications of switching reagent ions in proton transfer reaction mass spectrometric instruments for the improved selectivity of explosive compounds, Int. J. Mass Spectrom. 354-355 (2013) 123–128, https://doi.org/10.1016/j.ijms.2013.05.004.
[31] F.C. Fehsenfeld, M. Mosesman, E.E. Ferguson, Ion—molecule reactions in an O 2 +—H 2 O system, J. Chem. Phys. 55 (1971) 2115–2120, https://doi.org/10.1063/1.1676382.
[32] F.C. Fehsenfeld, M. Mosesman, E.E. Ferguson, Ion—molecule reactions in NO + —H 2 O system, J. Chem. Phys. 55 (1971) 2120–2125, https://doi.org/10.1063/1.1676383.
[33] E.E. Ferguson, Ion-molecule reactions in the atmosphere, in: P. Ausloos (Ed.), Kinetics of Ion-Molecule Reactions, Springer US, Boston, MA, 1979, pp. 377–403.
[34] E.E. Ferguson, F. Arnold, Ion chemistry of the stratosphere, Acc. Chem. Res. 14 (1981) 327–334, https://doi.org/10.1021/ar00071a001.
[35] E.E. Ferguson, F.G. Fehsenfeld, D.L. Albritton, Ion Chemsitry of the Earth's Atmosphere, Gas Phase Ion Chemistry, 1979.
[36] M.M. Shahin, Use of corona discharges for the study of ion—molecule reactions, J. Chem. Phys. 47 (1967) 4392–4398, https://doi.org/10.1063/1.1701643.
[37] J. Langejuergen, M. Allers, J. Oermann, A. Kirk, S. Zimmermann, Quantitative detection of benzene in toluene- and xylene-rich atmospheres using high-kinetic-energy ion mobility spectrometry (IMS), Anal. Chem. 86 (2014) 11841–11846, https://doi.org/10.1021/ac5034243.
[38] J. Dumas, P. Dupuis, G. Pfister Guillouzo, C. Sandorfy, Ionization Potentials and Ultraviolet Absorption Spectra of Fluorocarbon Anesthetics, twenty-sixth.-Third, CAN. J. SPECTROS, 1981.
[39] M. Müller, F. Piel, R. Gutmann, P. Sulzer, E. Hartungen, A. Wisthaler, A novel method for producing NH4+ reagent ions in the hollow cathode glow discharge ion source of PTR-MS instruments, Int. J. Mass Spectrom. 447 (2020) 116254, https://doi.org/10.1016/j.ijms.2019.116254.
[40] E.G. Nazarov, S.L. Coy, E.V. Krylov, R.A. Miller, G.A. Eiceman, Pressure effects in differential mobility spectrometry, Anal. Chem. 78 (2006) 7697–7706, https://doi.org/10.1021/ac061092z.
[41] O. Anttalainen, E. Lattouf, T. Kotiaho, G. Eiceman, Ion density of positive and negative ions at ambient pressure in air at 12-136 mm from 4.9 kV soft x-ray source, Rev. Sci. Instrum. 92 (2021) 54104, https://doi.org/10.1063/5.0050669.
[42] B.C. Hauck, C.S. Harden, V.M. McHugh, Isoflurane as an accurate negative mode calibrant for ion mobility spectrometry, Anal. Chem. (2021), https://doi.org/10.1021/acs.analchem.1c03894.
[43] R. González-Méndez, P. Watts, D.C. Howse, I. Procino, H. McIntyre, C.A. Mayhew, Ion mobility studies on the negative ion-molecule chemistry of isoflurane and enflurane, J. Am. Soc. Mass Spectrom. 28 (2017) 939–946, https://doi.org/10.1007/s13361-017-1616-0.